

Unsupervised Extraction of Degradation Related Features from Battery Cycling Data via a Conditional Temporal Convolutional Autoencoder

Jianxiang Wang¹, Shijie Weng¹, Xuesong Feng¹, Xiaoli Peng¹, Yong Xiang^{1*}

¹ School of Materials and Energy, University of Electronic Science and Technology of China, Chengdu, China (*Corresponding Author)

ABSTRACT

Clean energy production is often accompanied by battery storage systems that undergo complex degradation processes. Incremental capacity and differential voltage peaks are traditionally used for degradation analysis, but are sensitive to current rate, deep degradation, and battery chemistry. To enhance the robustness of degradation feature tracking, this study proposes a conditional temporal convolutional autoencoder. The unsupervised nature of the proposed method enables the extraction of degradation related features from data that have no peak features. Results show that the proposed method can extract features and reconstruct battery cycling curves with high fidelity. Furthermore, the extracted features are highly correlated with peak locations of incremental capacity and differential voltage curves. The extracted features also have less noise and no missing values compared to the peak locations. Prediction of peak locations from single encoding achieves mean absolute errors of 0.019 V and 2.4% state-of-charge. The proposed method is therefore potentially useful for battery degradation analysis and health assessment.

Keywords: lithium-ion battery, differential voltage analysis, incremental capacity analysis, neural network, unsupervised learning

NONMENCLATURE

Abbreviations

ADAM	Adaptive moment estimation
ANN	Artificial neural network
CC	Constant current
CPU	Central processing unit

CTCA	Conditional temporal convolutional autoencoder
CV	Constant voltage
DCA	Deep convolutional autoencoder
DVA	Differential voltage analysis
GPU	Graphic processing unit
ICA	Incremental capacity analysis
LIB	Lithium-ion battery
MAE	Mean absolute error
RAM	Random access memory
RUL	Remaining useful life
SOC	State-of-charge

1. INTRODUCTION

LIBs have become widely used in consumer electronics [1, 2], transportation [3, 4], and energy storage [1, 5] due to their high energy density, power density, and relatively long lifetime. LIBs are considered especially promising as an energy storage component in clean and sustainable energy production for the regulation of uncertain power demands and renewable power supplies such as solar and wind [6]. However, LIBs degrade after extended usage due to factors including the depth of discharge, current load, and external temperature [6], which leads to reduced battery performance. Therefore, an accurate understanding of the degradation mechanism of LIBs is crucial to the development of high-performance battery materials and sustainable energy systems.

Previous studies used ICA and DVA to reveal the underlying mechanism of battery degradation. In ICA and DVA, the peak features of differential cycling curves are related to the battery intercalation process and correspond to degradation modes such as loss of lithium inventory and loss of active materials [7, 8]. Due to the peaks' correlation with degradation modes, many

studies also used ICA and DVA for battery health estimation [9, 10], degradation mode estimation [7, 11], and RUL prediction [12]. However, real battery usage often involves deep degradation and high current rate cycling, for which ICA and DVA are less effective due to the loss of peak features [13].

Recent studies have shown that ANNs can accurately predict battery capacity from cycling conditions [14] and can produce accurate battery health estimation [15], degradation mode estimation [11], and RUL prediction [16] based on ICA and DVA. However, these studies involved supervised training of ANNs which requires target data produced by ICA and DVA. Incorrect or missing target data caused by these analyses therefore adversely affect the training process, which makes supervised ANNs less applicable to cycling data of varied current rates, degradation levels, and battery chemistries.

Previous studies have successfully used DCAs for unsupervised feature extraction of high-dimensional data such as two-dimensional images [17]. We thus hypothesize that DCAs can similarly extract degradation related features from one-dimensional battery cycling curves. Nevertheless, few existing studies have investigated the application of DCAs to the extraction of degradation features. Therefore, this study proposes a CTCA for degradation feature extraction from battery cycling data, and analyzes the relationship between extracted features and peak locations of incremental capacity and differential voltage curves.

2. BATTERY CYCLING TESTS

To provide data for the training of CTCA, cycling data of 2025-format batteries assembled in lab experiments were collected. The 2025-format batteries were assembled from $\text{LiNi}_{0.8}\text{Co}_{0.1}\text{Mn}_{0.1}\text{O}_2$ cathodes, lithium metal anodes, and electrolytes based on LiPF_6 , various carbonate esters, and other additives. The batteries had a nominal capacity of 1.6 mAh, and were cycled at different charging and discharging rates between 3 to 4.2 V using LANHE CT3001A 5V 20mA or 50mA battery testing systems. All tests were conducted in a temperature-controlled room at $25 \pm 1^\circ\text{C}$. Table 1 lists the detailed test setup. The CC charging and discharging

Table 1 Test setup of the 2025-format batteries

Number of batteries	Charging method	Discharging method	Number of CC steps
63	1 C, CC-CV	1 C, CC	120,217
28	1 C, CC	1 C, CC	
75	5 C, CC-CV	0.5 C, CC	
27	6 C, CC	0.5 C, CC	

steps of the tests were used for peak and feature extraction.

3. FEATURE EXTRACTION METHODS

3.1 Conditional Temporal Convolutional Autoencoder

Based on the lack of known target values, a DCA is needed for the feature extraction problem of this study. A DCA takes high-dimensional data such as images or sequences as input, reduces the data to low-dimensional encodings, and reconstructs the original data from these encodings. This approach ensures the DCA learns an effective low-dimensional representation of the original data without using target values. Therefore, a DCA-based CTCA is used for cycling curve feature extraction.

The CTCA is a modification of the conditional temporal convolutional encoder-decoder proposed by the authors for battery capacity prediction [14]. Fig. 1c shows the structure of the CTCA which includes the target encoder, condition encoder, and decoder. The target encoder extracts the voltage curve features of a charging or discharging step using the voltage, sampling interval, and current rate as inputs. The condition encoder and decoder reconstruct the original voltage curve from these features using the sampling interval and current rate as inputs. To reconstruct the voltage curve with full information of the sampling interval and current rate, the condition encoder and decoder layers are interconnected. The CTCA uses causal convolution to

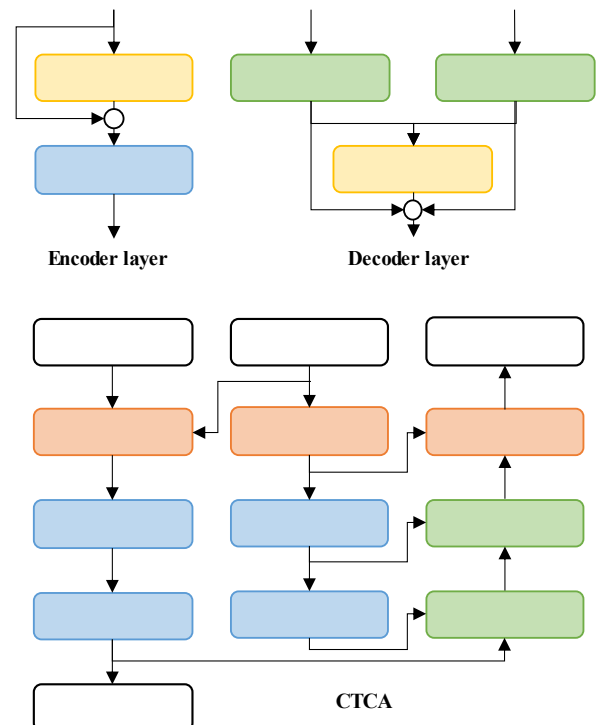


Fig. 1. The structure of (a) encoder layers, (b) decoder layers, and (c) high-level structure of CTCA.

Table 2 Training parameters of CTCA

	Parameter	Value
Dataset	Batch size	64
	Training set ratio	80%
	Validation set ratio	10%
	Test set ratio	10%
CTCA	Number of channels	16
	Number of layers	5
	Convolution window size	4
	L2 regularization	1×10^{-6}
	Artificial voltage noise (V)	$\mathcal{N}(0, 0.01)$
Training	Method	ADAM
	Learning rate	0.005–0.0001
	1st and 2nd moment decay	0.5, 0.999
	Loss function	MAE
	Epochs	100

model the temporal effects of the input conditions. In causal convolution, inputs of the convolution (Fig. 1a and Fig. 1b) and average-pooling layers (Fig. 1a) are right-padded with zero values. Similarly, outputs of the up-sampling layers (Fig. 1b) are right-truncated so that the next decoder or linear layers (Fig. 1c) have two inputs of equal lengths. The average-pooling size and up-sampling size are equal to the convolution window size.

The CTCA was trained with the charging and discharging steps of the 2025-format batteries. Each step was down-sampled to less than 1000 samples to improve training speed. The steps were randomly split into training, validation, and test sets. L2 regularization was used and normal-distributed artificial voltage noise was added to the input during training to improve model generalization. The learning rate was halved when evaluation loss plateaus for 5 epochs to improve training. The training was performed with TensorFlow on an NVIDIA GeForce RTX 2080 Ti GPU with 11 GB RAM and an Intel Core i9-10900X CPU with 128 GB RAM.

Table 2 lists the training parameters of CTCA. The validation and test set ratios were chosen to be small due to the abundance of data. The number of channels were chosen to be small to limit encoding size and prevent overfitting. The number of layers and convolution window size were chosen to achieve a receptive field of 1024 samples. Other parameters were selected empirically, but a systematic search is out of the scope of this paper.

3.2 Baseline peak extraction method

Past studies have investigated the tracking of differential curve peaks without [18] or with filters [7] and the tracking of a single peak using support vector regression [8, 9]. However, these studies did not address the robustness of multiple peak tracking when some

peak features are lost to degradation or when peak signature changes across different battery chemistries. Therefore, this study uses a peak tracking method with improved robustness and agnostic of battery chemistry to allow for an analysis of the relationship between the peaks and CTCA encodings through the entire battery life. The method extracts the differential curve peaks by using smoothed derivatives and linear sum assignment-based target tracking.

First, the derivatives of the capacity-voltage curve of a step are calculated. For DVA, the derivatives of V with respect to Q is calculated, whereas for ICA, the derivatives of Q with respect to V is calculated, where V is the voltage and Q is accumulative charging or discharging capacity. The peak locations of a step are then extracted by finding the sample points where a zero-crossing of the second derivative and a sufficiently large negative value of the third derivative is found, as shown in (1), where x and y are V and Q for DVA and Q and V for ICA, respectively, $\sigma = 1$ (charging) or $\sigma = -1$ (discharging), t is the sample index, N is the sample count, $t \in [1, N]$, and T_d is the third derivative threshold.

$$P' = \left\{ x_t \left[\begin{array}{l} \sigma \frac{d^2 y}{dx^2} \Big|_{\max(t-1,1)} \geq 0, \sigma \frac{d^2 y}{dx^2} \Big|_{\max(t+1,N)} \leq 0, \\ \sigma \frac{d^3 y}{dx^3} \Big|_t \leq -T_d \left\{ \max \left(\frac{d^3 y}{dx^3} \right) - \min \left(\frac{d^3 y}{dx^3} \right) \right\} \end{array} \right. \right\} \quad (1)$$

Peaks too close to other peaks are then removed, as shown in (2), where T_x is the peak distance threshold.

$$P = \{p'_j \in \text{sorted}(P') \mid j = 1 \text{ or } p'_j - p'_{j-1} \geq T_x\} \quad (2)$$

The smoothed derivatives are calculated with a half-window size of w by applying (3) recursively.

$$\frac{d\hat{y}_t}{dx_t} = \frac{y_{\min(t+w,N)} - y_{\max(t-w,1)}}{x_{\min(t+w,N)} - x_{\max(t-w,1)}} \quad (3)$$

The method then tracks the peaks of the cycling steps using linear sum assignment with a heuristic cost matrix considering that the peak locations almost always change gradually during degradation. This process produces several traces, each containing the peaks that are most likely the same physical peak. For peak $p_{k,j}$ at cycling step k , the cost matrix M satisfies (4), where \hat{p}_i is the smoothed peak location of trace i , $k_{\text{last},i}$ is the last step number of trace i , L_i is the number of peaks in trace i , and α and β are penalty multipliers for non-continuous or short traces. This cost matrix ensures that peaks are assigned to the closest trace in most cases and the traces are as continuous as possible.

$$M = \{m_{j,i}\} = \{p_{k,j} - \hat{p}_i + \alpha(k - k_{\text{last},i}) + \beta/L_i\} \quad (4)$$

Algorithm 1 Peak curve extraction

Inputs: N_s : number of steps, m_k : number of peaks at step k , $k \in [1, N_s]$, $p_{k,j}$: location of peak j at step k , $j \in [1, m_k]$, and γ : peak smoothing rate.

Outputs: N_c : number of traces, K_i : step indices of trace i , $i \in [1, N_c]$, and P_i : peak locations of trace i .

```

1:  $N_c := 0$ 
2: foreach  $k \in [1, N_s]$  do
3:   Calculate the cost matrix  $M$ .
4:   Solve the linear sum assignment problem represented
   by  $M$  to obtain zero or one peak index  $j_i$  assigned
   to each trace  $i$ .
5:   // Assigned peaks
6:   foreach  $i \in [1, N_c]$  do
7:     if  $j_i$  exists then
8:        $\hat{p}_i := \gamma \hat{p}_i + (1 - \gamma)p_{k,j_i}$ ,  $k_{\text{last},i} := k$ ,  $L_i := L_i + 1$ ,
        $K_i := (K_i \ k)$ , and  $P_i := (P_i \ p_{k,j_i})$ 
9:     end if
10:  end for
11:  // Unassigned peaks
12:  foreach  $j \in [1, m_k]$  do
13:    if  $j \notin \{j_i\}$  then
14:       $N_c := N_c + 1$ ,  $\hat{p}_{N_c} := p_{k,j}$ ,  $k_{\text{last},N_c} := k$ ,  $L_{N_c} := 1$ ,
       $K_{N_c} := (k)$ , and  $P_{N_c} := (p_{k,j})$ 
15:    end if
16:  end for
17: end for
18: Remove  $K_i$  and  $P_i$  if the length is lower than  $N_s/4$ 
to filter out unusable traces.

```

Algorithm 1 and Table 3 show the pseudo-code and the empirically chosen parameters of the method.

4. RESULTS AND DISCUSSION

4.1 Autoencoder accuracy

The CTCA performs well on all cycling data of this study. Fig. 2 shows battery voltage curves at different current rates in the test set and the corresponding voltage curves reconstructed by CTCA. The reconstruction error is generally low and important features such as voltage platforms are preserved. The error slightly increases at the start and end of some curves and in high-rate steps, but these locations usually do not contain peak features, so the error's influence on the CTCA encodings' relationship with peaks is minimal. Furthermore, the MAE of the CTCA on the test set is 8.5 mV or about 0.7% of the 3 to 4.2 V interval. This high-fidelity reconstruction is promising for the correct extraction of degradation related features.

4.2 Comparison of peaks and encodings

Fig. 3 shows the peaks extracted by the baseline method from a 1 C cycling test. The method correctly

Table 3 Parameters of the baseline method

Parameter	Value
3rd derivative threshold T_d	1×10^{-2}
Peak distance threshold T_x	5×10^{-2}
1st derivative half-window size w	8
2nd derivative half-window size w	8
3rd derivative half-window size w	16
Non-continuity penalty α	5×10^{-2}
Low-length penalty β	5×10^{-1}
Peak smoothing rate γ	0.9

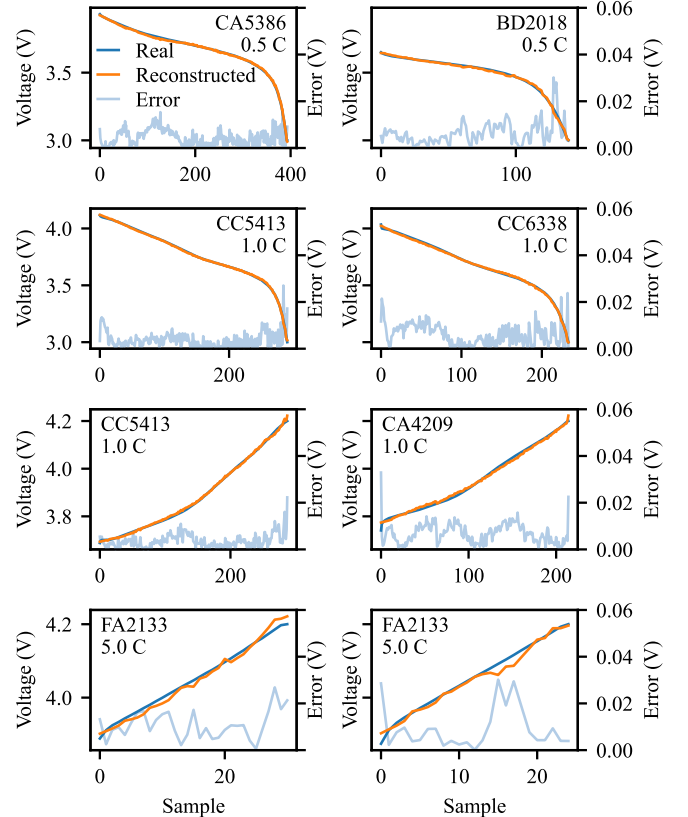


Fig. 2. Real voltage curves and CTCA reconstruction at different current rates.

extracts the main peaks in the curves and ignores small peaks caused by measurement noise. However, the differential curves lose peak features after degradation. For example, step 4 has two dV/dQ peaks (Fig. 3a) and three dQ/dV peaks (Fig. 3c) and step 13 has three dV/dQ peaks (Fig. 3b) and three dQ/dV peaks (Fig. 3d). In contrast, step 454 only has one dQ/dV peak (Fig. 3c) and step 463 loses all peak features (Fig. 3d). The baseline method therefore becomes less reliable after battery degradation.

The baseline peak extraction method and the CTCA was then applied to the full cycling tests. For most of the cycles, the baseline method can extract the peaks of dQ/dV (Fig. 4a and Fig. 4c) and dV/dQ (Fig. 4b) curves correctly. However, when batteries are degraded, the baseline method is less reliable as the differential curves

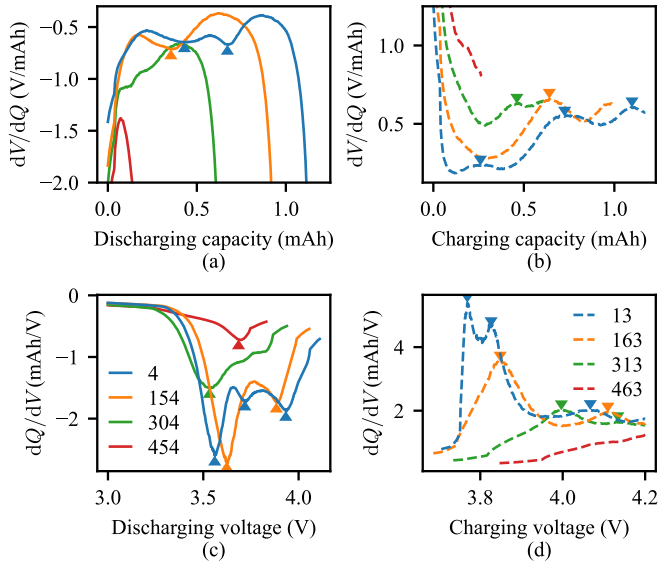


Fig. 3. Peaks extracted by the baseline method from the (a, b) dV/dQ and (c, d) dQ/dV curves of battery A12041 cycled at 1 C.

lose features. The baseline method also fails to extract usable dV/dQ peaks from a battery charged at 5 C (Fig. 4c) due to the lack of peak features. These feature losses preclude the training of supervised ANNs based on known target values. In contrast, the CTCA produces encodings regardless of the degradation level and current rate. These encodings can then be related to the peaks and used for reliable degradation feature extraction.

To explore the relationship between the peaks and CTCA encodings, for each peak, a closest encoding was found by calculating the R^2 (coefficient of determination) of linear regression between the encodings and the peak. The encoding with the highest R^2 value was considered the closest and fitted with linear regression to predict the peak. For dV/dQ peaks, the linear regression was performed with the SOC values corresponding to the peak locations according to (5) so that the regression is less affected by the peak's correlation with capacity. In (5), SOC_t is the SOC at sample t , C_t is the accumulative charging or discharging capacity at sample t , and C is the total charging or discharging capacity.

$$SOC_t = \begin{cases} \frac{C_t}{C} & \text{if charging,} \\ 1 - \frac{C_t}{C} & \text{if discharging.} \end{cases} \quad (5)$$

Fig. 4 compares the peaks extracted by the baseline method and the corresponding prediction by encodings. The prediction shows a surprising resemblance to actual peak traces, does not have missing values, and has less noise compared to the peak traces. In Fig. 4c, the encodings also capture the long-term turbulence of the

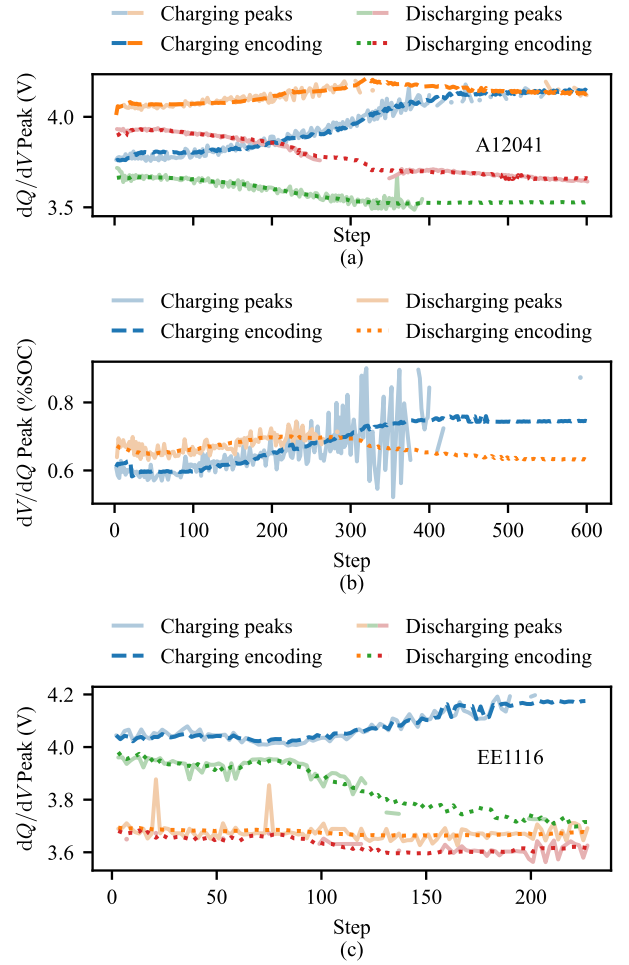


Fig. 4. Peaks extracted using the baseline method and the closest prediction from single encoding using linear regression. (a) dQ/dV and (b) dV/dQ peaks of battery A12041 (1 C cycling) and (c) dQ/dV peaks of battery EE1116 (5 C charging, 0.5 C discharging).

peaks near 4.0 V before step 100. The MAEs between the peaks and the prediction by encodings of all batteries are 0.019 V for dQ/dV peaks and 2.4% SOC for dV/dQ peaks, which are small compared to the voltage and SOC ranges. These results show that the CTCA can produce encodings related to the peaks without supervised training, and these encodings can be more reliable in the analysis of degradation and estimation of battery health.

In Fig. 4a, the dQ/dV peaks are initially near 4.0 V and 3.7 V, but an increase in polarization during aging causes the peak locations to diverge from these two voltage values. Nevertheless, the distance between the peaks decreases in both charging and discharging curves. Because the peak locations of the half-cell without polarization should stay relatively constant during aging, this seems to suggest that the polarization increases more during discharging at higher voltage and charging at lower voltage compared to discharging at lower voltage and charging at higher voltage. In Fig. 4c, the

discharging dQ/dV peak initially near 4.0 V decreases faster in the predicted part after step 120 than the charging peak increases, which is consistent with this observation. In Fig. 4b, the dV/dQ peaks slightly shift towards higher SOC during aging, possibly because the increase of polarization causes charging to be cut off earlier at high voltage than discharging is cut off at low voltage.

5. CONCLUSION

This paper proposes a CTCA for the extraction of degradation related features from battery cycling data. The extracted CTCA encodings highly resemble the peak locations of incremental capacity and differential voltage curves, but are more stable and less noisy compared to the peaks. Prediction of peak locations from single encoding achieves MAEs of 0.019 V and 2.4% SOC. Because the features of battery cycling curves often reflect the evolution of battery degradation modes, an accurate extraction of these features allows a precise analysis of battery degradation, which can in turn enable the development of higher-performance battery materials and more sustainable energy systems. Future work should therefore investigate the relationship between the CTCA encodings and measured battery degradation modes and explore the assessment of battery health using these encodings.

ACKNOWLEDGEMENT

We thank Professor Jingjing Li for helpful suggestions.

REFERENCES

- [1] Stroe DI, Swierczynski M, Stroe AI, Kaer S, Teodorescu R. Lithium-ion battery power degradation modelling by electrochemical impedance spectroscopy. *IET Renew Power Gen*, 2022;11(9):1136-1141.
- [2] Kabir MM, Demirocak DE. Degradation mechanisms in Li-ion batteries: a state-of-the-art review. *Int J Energ Res*, 2017;41:1963-1989.
- [3] Pastor-Fernández C, Yu TF, Widanage WD, Marco J. Critical review of non-invasive diagnosis techniques for quantification of degradation modes in lithium-ion batteries. *Renew Sust Energ Rev*, 2019;109:138-159.
- [4] Tian H, Qin P, Li K, Zhao Z. A review of the state of health for lithium-ion batteries: Research status and suggestions. *J Clean Prod* 2020;261:120813.
- [5] Xu B, Oudalov A, Ulbig A, Andersson G, Kirschen DS. Modeling of lithium-ion battery degradation for cell life assessment. *IEEE T Smart Grid* 2016;9(2):1131-1140.
- [6] Ahmadian A, Sedghi M, Elkamel A, Fowler M, Golkar MA. Plug-in electric vehicle batteries degradation modeling for smart grid studies: Review, assessment and conceptual framework. *Renew Sust Energ Rev* 2018;81:2609-2624.
- [7] Chen J, Marlow MN, Jiang Q, Wu B. Peak-tracking method to quantify degradation modes in lithium-ion batteries via differential voltage and incremental capacity. *J Energy Storage* 2022;45:103669.
- [8] Weng C, Feng X, Sun J, Peng H. State-of-health monitoring of lithium-ion battery modules and packs via incremental capacity peak tracking. *Appl Energ* 2016;180:360-368.
- [9] Weng C, Cui Y, Sun J, Peng H. On-board state of health monitoring of lithium-ion batteries using incremental capacity analysis with support vector regression. *J Power Sources* 2013;235:36-44.
- [10] Li X, Yuan C, Wang Z. State of health estimation for Li-ion battery via partial incremental capacity analysis based on support vector regression. *Energy* 2020;203:117852.
- [11] Lee S, Kim Y. Li-ion battery electrode health diagnostics using machine learning. *Amer Contr Conf* 2020:1137-1142.
- [12] Li X, Wang Z, Yan J. Prognostic health condition for lithium battery using the partial incremental capacity and Gaussian process regression. *J Power Sources* 2019;421:56-67.
- [13] Fly A, Chen R. Rate dependency of incremental capacity analysis (dQ/dV) as a diagnostic tool for lithium-ion batteries. *J Energy Storage* 2020;29:101329.
- [14] Wang J, Xiang Y. Fast modeling of the capacity degradation of lithium-ion batteries via a conditional temporal convolutional encoder-decoder. *IEEE T Transp Electr*, in press.
- [15] She C, Wang Z, Sun F, Liu P, Zhang L. Battery aging assessment for real-world electric buses based on incremental capacity analysis and radial basis function neural network. *IEEE T Ind Inform* 2020;16(5):3345-3354.
- [16] Zhang S, Zhai B, Guo X, Wang K, Peng N, Zhang X. Synchronous estimation of state of health and remaining useful lifetime for lithium-ion battery using the incremental capacity and artificial neural networks. *J Energy Storage* 2019;26:100951.
- [17] Cheng Z, Sun H, Takeuchi M, Katto J. Deep convolutional autoencoder-based lossy image compression. *Picture Coding Symposium* 2018:253-257.
- [18] Maures M, Capitaine A, Delétage JY, Vinassa JM, Briat O. Lithium-ion battery SOH estimation based on incremental capacity peak tracking at several current levels for online application. *Microelectron Reliab* 2020;114:113798.